ChemComm

FEATURE ARTICLE

View Article Online
View Journal | View Issue

Cite this: *Chem. Commun.*, 2025, **61**, 5719

Impact of harmful ions in seawater on electrolysis catalysts: challenges and mitigation strategies

Hanxiao Du,[abc] Tongming Sun,[d] Minmin Wang,[d] Yanfeng Tang,[d] Yang Yu*[e] and Jiacheng Wang *[abf]

Direct seawater electrolysis presents a promising solution to address both freshwater scarcity and the growing demand for green hydrogen in regions abundant in renewable energy. This study first investigates the electrochemical mechanisms of seawater electrolysis, decomposing the process into cathodic and anodic reactions. It then reviews the impact of seawater's complex ionic composition on electrocatalyst performance, focusing on activity, selectivity, and stability. The challenges posed by anionic interference from Cl^- and Br^-, and cationic interference from Mg^{2+} and Ca^{2+}, are discussed, along with effective mitigation strategies. Solutions to mitigate the impact of anions on the anode, such as heterojunction engineering, nanostructure design and constructing anti-corrosion layers, are proposed. Anodic small molecule oxidation is employed as an alternative to the oxygen evolution reaction (OER) to decrease the overall energy consumption. For the cationic interference on the cathode, strategies like maintaining the hydrophobicity of the electrode and electrolysis cell design are suggested. Finally, this review summarizes the remaining challenges, presents feasible solutions, and highlights key considerations for scaling up seawater electrolysis for commercial hydrogen production. This review provides valuable insights to accelerate the development of sustainable, large-scale seawater hydrogen production technologies.

Received 16th February 2025,
Accepted 14th March 2025

DOI: 10.1039/d5cc00844a

rsc.li/chemcomm

1. Introduction

The sustainable development of hydrogen energy is crucial for achieving the strategic goals of 'carbon peaking and carbon neutrality'. Green hydrogen production and efficient utilization through water electrolysis technology form a truly recyclable clean energy system with carbon zero-emission. For the commonly available commercial water electrolyzers, the pure water feed is achieved through an external seawater desalination plant's pretreatment and purification process or by integrating the electrolyzer system with a seawater purification system (such as reverse osmosis). This reduces the overall robustness of the water electrolyzer system, requiring additional costs for frequent equipment maintenance. Furthermore, the development potential of green hydrogen is directly linked to the cost of sustainable energy.[1] Thus, establishing large-scale hydrogen production facilities in regions rich in sustainable energy is an ideal low-cost approach for green hydrogen production.[2] However, these regions are generally located in offshore or desert areas, which are severely lacking in freshwater resources, limiting the industrialization of green hydrogen by water electrolysis.[3,4] For instance, Australia has abundant solar energy resources in coastal areas where the annual solar irradiation totally ranges from 7621 to 8672 MJ m^{-2}. Nonetheless, these regions are extremely scarce in freshwater resources. Therefore, establishing direct seawater electrolysis systems in such areas can provide a feasible solution for large-scale green hydrogen production, prompting an explosive growth in research on direct seawater electrolysis for hydrogen production.[5–7]

Direct seawater electrolysis offers a feasible solution, as it avoids the need for water purification systems, reduces system complexity, and lowers capital and maintenance costs. This approach is particularly valuable for large-scale hydrogen production. Furthermore, the ocean economy, with its low-cost marine transportation, renewable energy resources, and existing offshore oil and gas infrastructure, provides an ideal platform for direct seawater electrolysis development. Deploying such

[a] *Zhejiang Key Laboratory for Island Green Energy and New Materials, Institute of Electrochemistry, School of Materials Science and Engineering, Taizhou University, Taizhou, 318000, Zhejiang, China. E-mail: jiacheng.wang@tzc.edu.cn*
[b] *State Key Laboratory of High-Performance Ceramics and Superfine Microstructure, Shanghai Institute of Ceramics, Chinese Academy of Sciences, Shanghai, 200050, China*
[c] *Center of Materials Science and Optoelectronics Engineering, University of Chinese Academy of Sciences, Beijing, 100049, China*
[d] *College of Chemistry and Chemical Engineering, Nantong University, Nantong, 226019, China*
[e] *School of Pharmaceutical Sciences, Taizhou University, Taizhou, 318000, Zhejiang, China. E-mail: yuyang430@tzc.edu.cn*
[f] *Key Laboratory of Advanced Energy Materials Chemistry (Ministry of Education), Nankai University, Tianjin, 300071, China*

infrastructure can reduce carbon emissions from marine transport, create new industries, and generate job opportunities, promoting the blue economy.[8] Additionally, seawater used in hydrogen production generates freshwater, which can be directly utilized or used to recharge saline aquifers, benefiting farming and freshwater fisheries in remote areas. However, the complex composition of seawater, with various ions significantly affecting the catalyst, presents a major challenge. Generally, the total salt concentration in seawater is 3.5 wt%, with 11 kinds of ions having a concentration greater than 0.0005 mol L^{-1}. Among them, Cl^- is 0.5658 mol L^{-1}, SO_4^{2-} is 0.0293 mol L^{-1}, Br^- is 0.0009 mol L^{-1}, Na^+ is 0.4862 mol L^{-1}, Mg^{2+} is 0.0548 mol L^{-1}, Ca^{2+} is 0.0105 mol L^{-1}, K^+ is 0.0106 mol L^{-1}, $B(OH)_3^-$ is 0.0003 mol L^{-1}, $B(OH)^{4-}$ is 0.0001 mol L^{-1}, HCO_3^- is 0.0018 mol L^{-1}, and CO_3^{2-} is 0.0003 mol L^{-1}. It is necessary not only to inhibit the influence of anions on seawater electrolysis, but also to prevent cationic precipitation.[9] Thus, direct seawater electrolysis for hydrogen production is still in its early research stages, and the impact of the complex composition of seawater on the electrolysis process has not been fully understood. In the process of natural seawater electrolysis, molybdenum nitride (Mo_2N) catalysts have been utilized to address key challenges. During the reaction, ammonium (NH_4^+) cations are generated *in situ* on the catalyst surface. These cations form hydrogen bonds with hydroxyl groups (OH^-) produced from the dissociation of interfacial water molecules, effectively suppressing hydroxide formation. Additionally, the NH_4^+ groups significantly enhance the hydrogen-bonding network connectivity within the electric double layer (EDL), reducing hydrogen transfer barriers and thereby improving the energy efficiency of hydrogen-related reactions.[10] Yang *et al.* proposed a protective strategy by introducing V_2O_3 layers for *in situ* reduction in a low-supported catalyst of platinum and nickel.[11] A Lewis acid V_2O_3 layer can store excessive OH^- ions, and reduce Cl^- corrosion and alkaline earth salt precipitation during electrolysis.

To address this challenge, we decompose the electrolysis process into cathodic and anodic reactions and review the influence of different ions in seawater on different electrodes, as well as existing solutions. We systematically review the impact of various ions on different electrodes and evaluate existing mitigation strategies. Advanced approaches such as the rational design of selective electrocatalysts and innovative system architectures are proposed to address ionic interference and enhance efficiency and durability. Finally, we summarize the challenges of seawater electrolysis, propose potential solutions, and highlight key considerations for achieving commercial hydrogen production from seawater electrolysis in the future. We hope this work provides valuable insights to advance the commercialization of seawater electrolysis.

2. Competing the OER with the chlorine evolution reaction (ClER) in seawater electrolysis

The principle of hydrogen production by seawater electrolysis is similar to that of hydrogen production by freshwater electrolysis, which is a 2-proton coupled electron process of the hydrogen evolution reaction (HER) at the cathode. These reactions can be expressed under acidic and alkaline conditions by eqn (1) and (2):[10,12–15]

- Acidic:

$$2H^+ + 2e \rightarrow H_2\uparrow \quad (1)$$

- Alkaline

$$2H_2O + 2e \rightarrow H_2\uparrow + 2OH^- \quad (2)$$

Compared to the HER, the OER is a more complex process involving 4-electron transfer, leading to a high energy barrier that reduces the overall efficiency of seawater electrolysis. The OER equations in acidic and alkaline electrolytes are as follows:

- Acidic:

$$2H_2O \rightarrow 4H^+ + O_2\uparrow + 4e^- \quad (3)$$

- Alkaline:

$$4OH^- \rightarrow 2H_2O + O_2\uparrow + 4e^- \quad (4)$$

The effects of these components on the cathode and anode catalysts are deduced based on the composition of seawater. Cl^- is the main factor affecting the anodic OER process in seawater electrolysis. Dionigi *et al.* proposed the use of Pourbaix diagrams to gain insight into the anodic reactions of seawater electrolysis,[16] specifically the chlorine evolution reaction (ClER) and oxygen evolution reaction (OER). As shown in Fig. 1a, when the pH value is less than 3.0, the ClER dominates over the OER. Thermodynamically, the standard electrode potential (E^θ) for the ClER is independent of pH and higher than that of the OER. At high anodic potentials and pH values between 3 and 7.5, hypochlorous acid (HClO) formation becomes the primary reaction. Since the OER potential is pH-dependent and decreases with increasing pH, the potential difference between the OER and ClER increases with pH. When the pH exceeds 7.5, hypochlorite formation (which competes with the OER at the anode) becomes relevant. Partial dissociation (chlorine dissolved in water) and disproportionation (hypochlorite subjected to high temperatures) complicate the chemistry of chlorine species. In different pH ranges (Fig. 1a), the corresponding chloride oxidation can be represented by the following equations:[16–19]

$$2Cl^- \rightarrow Cl_2 + 2e \quad (E^\theta = 1.36\ \text{V}\ \textit{vs.}\ \text{SHE, pH} = 0) \quad (5)$$

$$Cl^- + H_2O \rightarrow H^+ + 2HClO + 2e \quad (E^\theta = 1.494 - 0.0295 \times \text{pH V}\ \textit{vs.}\ \text{SHE}, 3 < \text{pH} < 7.5) \quad (6)$$

$$Cl^- + 2OH^- \rightarrow ClO^- + H_2O + 2e \quad (E^\theta = 1.795 - 0.0591 \times \text{pH V}\ \textit{vs.}\ \text{SHE, pH} > 7.5) \quad (7)$$

Although the OER is thermodynamically favored, the 2-electron transfer kinetics of the chloride reaction are faster than the 4-electron process of the OER. Maximizing the thermodynamic potential difference between these two reactions could result in a potential window with relatively high OER selectivity.

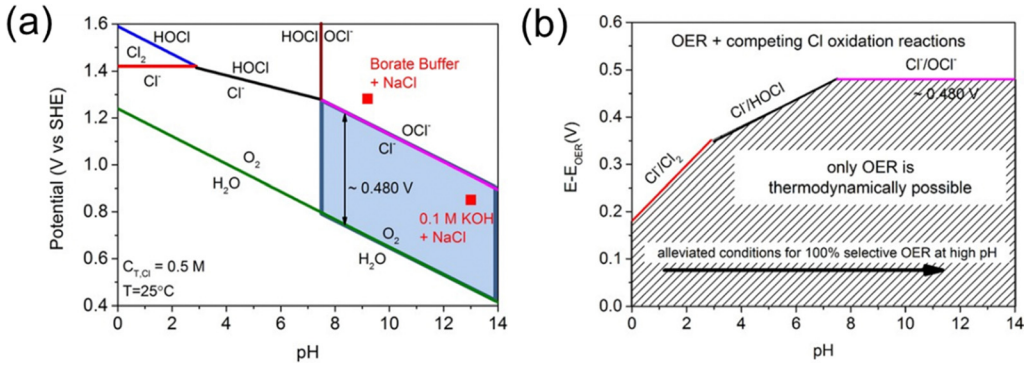

Fig. 1 (a) The Pourbaix diagram for the artificial seawater model. (b) Maximum allowed overpotential of OER electrolyzer catalysts in seawater. Values are obtained as a difference between the standard electrode potentials of the three relevant chloride oxidation reactions (chlorine, hypochlorous acid, and hypochlorite formation) and the OER *versus* pH.[16] Copyright © 2016 Wiley.

Within this potential window, an ideal electrocatalyst can generate a high OER current without forming hypochlorite.[20] As is shown in Fig. 1b, the potential difference (ΔE) increases with pH, reaching a maximum of 480 mV when pH > 7.5. The higher the pH, the easier it is to selectively split seawater. However, at high current densities (100–1000 mA cm^{-2}), the pH at the electrode surface may undergo significant changes, reducing the potential window for the selective OER. Moreover, competitive adsorption of Cl^- and OH^- at active sites within this potential window further complicates the process. Additionally, the competition between the ClER and OER limits the upper application potential of the anode, thereby hindering the development of high current density electrolyzers.[21]

3. Strategies for suppressing Cl^- corrosion in seawater electrolysis

The high concentration of Cl^- in seawater makes seawater electrocatalysis more challenging than freshwater or alkaline water electrolysis. Developing effective strategies to enhance the selectivity and activity of the OER while suppressing electrochemical reactions related to the ClOR is key to improving seawater electrolysis efficiency. Although traditional noble metal catalysts exhibit high catalytic activity, they are prone to corrosion in seawater environments, leading to a shortened lifespan.[22] Therefore, developing non-noble metal or alloy catalysts with high corrosion resistance has become a research focus. The improvement strategies for the anode catalysts in response to the influence of chloride ions mainly focus on three aspects: improving OER activity and selectivity, constructing chloride ion-blocking layers to suppress the ClOR, and biomass electrooxidation substituting the OER.[23] Common methods to enhance OER activity and selectivity include catalyst composition regulation, nanostructure design, and surface/interface modulation.[24–26]

3.1 Catalyst composition regulation

This is mainly achieved through doping for the formation of multi-metallic compounds. By doping with different metal or non-metal elements (*e.g.*, Fe, Co, Ni, Mn, Mo, P, S, *etc.*), the electronic structure of the catalyst can be adjusted, improving OER activity and selectivity. Designing multi-metallic compound catalysts (*e.g.*, bimetallic or multi-metallic oxides, alloys) optimizes the synergistic effects of active sites, thereby enhancing OER activity and selectivity.

For example, Li *et al.* used coordination polymer-derived epitaxial growth to construct a Ni–Fe MOF on $Ni(OH)_2$, which was then converted into phosphide (Fe–Ni_5P_4).[27] The decomposition of the MOF during the phosphorization process resulted in a layered, fluffy porous structure, creating Fe-doped Ni_5P_4 (Fe–Ni_5P_4) with high-density dispersed active sites. This structure facilitated electrolyte infiltration, exposing more active sites. A full water electrolysis cell using Fe–Ni_5P_4‖Fe–Ni_5P_4 achieved a high current density of 500 mA cm^{-2} with only 1.72 V of cell voltage and exhibited outstanding stability for 2700 hours. Even in alkaline seawater, the device maintained stable electrolysis at 1000 mA cm^{-2} for 1170 hours, as is shown in Fig. 2a and b. Similarly, Yang *et al.* synthesized RuCoBO multi-metallic nanocomposites (Ru_2Co_1BO-350) using a calcination method.[28] These exhibited excellent catalytic activity in the alkaline electrolysis of seawater for H_2 and O_2 production, with a HER overpotential of 14 mV and OER overpotential of 219 mV, coupled with low cell voltage (1.466 V@10 mA cm^{-2}) and long-term seawater electrolysis stability (230 hours@ 50 mA cm^{-2} and 100 mA cm^{-2}), as is depicted in Fig. 2c–e.

Additionally, Wang *et al.* combined wet impregnation and thermal annealing to prepare carbon-coated Ni-doped Fe_3N composite nanomaterials (Ni_x–Fe_3N@NCPs) (Fig. 2f).[29] PANI, with its unique π-conjugated structure and abundant nitrogen grafting sites, provided anchor points for Fe and Ni ions in the Fe/Ni–PANI precursor structure. The nitrogen-doped carbon coating in Ni_x–Fe_3N@NCPs enhanced conductivity, improved structural stability, and prevented the migration and aggregation of the active components of Ni_x–Fe_3N (Fig. 2g). The presence of nano-channel shielding effectively protected Ni_x–Fe_3N from corrosion by chloride ions. The incorporation of Ni atoms into Fe_3N adjusted the electronic configuration and induced lattice expansion, promoting reactant and intermediate adsorption and generating additional effective active sites. DFT calculations showed that Ni doping not only directed more electrons towards Fe

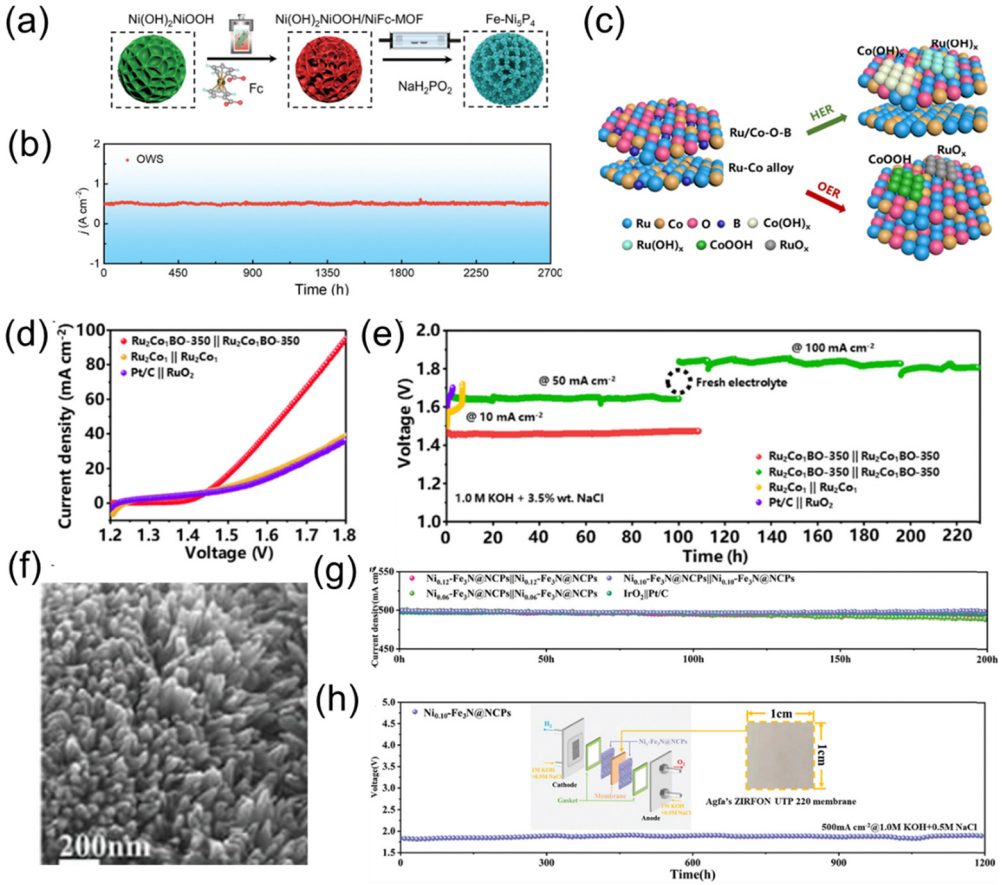

Fig. 2 (a) Schematic illustration of the synthesis process of Fe–Ni_5P_4. (b) Chronoamperometry curve of Fe–Ni_5P_4||Fe–Ni_5P_4 toward OWS at 500 mA cm^{-2}.[27] Copyright © 2024 Wiley-VCH GmbH. (c) Schematic illustration of the Ru_2Co_1BO-350 surface reconstructed in the HER and OER. (d) Polarization curves. (e) Long-term stability at current densities of 10, 50, and 100 mA cm^{-2}.[28] Copyright © 2023, American Chemical Society. (f) SEM images of $Ni_{0.10}$–Fe_3N@NCPs. (g) Time-dependent current density curves of Ni_x–Fe_3N@NCPs||Ni_x–Fe_3N@NCPs and IrO_2||Pt/C. (h) Voltage profile of zero-gap commercial electrolyzer with time at current densities of 500 mA cm^{-2}.[29] Copyright © 2024 Wiley-VCH GmbH.

centers, conferring higher conductivity, but also reduced reaction energy barriers, thus facilitating reaction kinetics. The optimal $Ni_{0.10}$–Fe_3N@NCPs catalyst required overpotentials of 47, 147, and 291 mV (HER) and 152, 249, and 312 mV (OER) to achieve current densities of 10, 100, and 500 mA cm^{-2}, respectively. In an alkaline seawater electrolyzer, only 1.8 V was needed to achieve 500 mA cm^{-2}, and no significant performance degradation was observed during 1200 hours of continuous electrolysis (Fig. 2h).

3.2 Nanostructure engineering

By precisely designing various nanostructures such as nanoparticles, nanowires, nanosheets, hollow structures, core–shell structures, and porous structures, the specific surface area of the catalyst can be significantly enhanced, fully exposing active sites. For instance, nanoparticle and nanowire structures increase specific surface areas and improve electron transport efficiency to enhance OER selectivity.[30,31] Hollow and porous structures optimize mass transfer dynamics and enhance active site utilization, accelerating reaction rates. Core–shell structures and layered double hydroxides (LDHs) utilize synergistic effects and interlayer distance modulation to further optimize catalyst stability and electronic structure. These nanostructure design strategies not only improve catalyst activity and stability but also provide new pathways for efficient energy conversion by precisely controlling the morphology and surface characteristics of materials.[32]

Zhang *et al.* optimized a Cr-doped Co_xP (Cr–Co_xP) electrocatalyst (Fig. 3a),[33] exhibiting excellent OER and HER activities. Experimental results and DFT calculations attributed the strong OER performance mainly to the work function release caused by Cr doping (Fig. 3b), which facilitated effective electron transfer between Cr–Co_xP and adsorbed oxygen species, reducing the energy barrier of the rate-determining step. In addition, the corrosion curve shown in Fig. 3c indicates that Cr–Co_xP has good long-term durability compared to Co_xP. Fei *et al.*[34] developed a core–shell nanoreactor consisting of NiFe alloy encapsulated in defect graphene layers (NiFe@DG) through a simple microwave shock strategy, acting as a high-performance OER catalyst (Fig. 3d and e). This catalyst achieved overpotentials of only 218 mV and 276 mV at 10 and 100 mA cm^{-2} in alkaline seawater, and its activity exhibited negligible decay (10%) after 2000 hours of continuous operation. Experimental and theoretical analyses revealed that the excellent durability of NiFe@DG was due to the formation of a

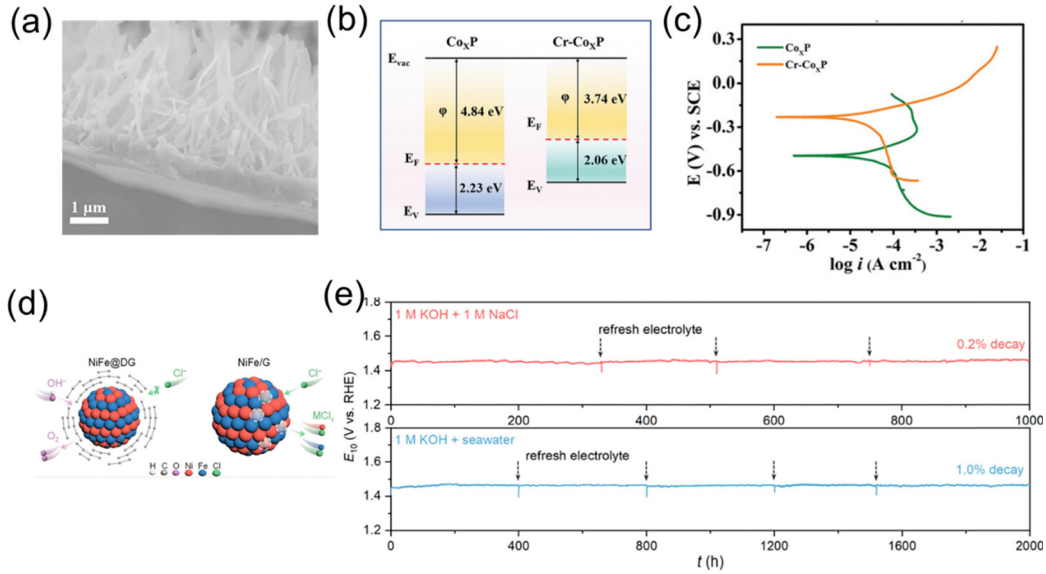

Fig. 3 (a) Cross-sectional SEM image of Cr–Co_xP. (b) Band structure alignment of the Co_xP and Cr–Co_xP. (c) Corrosion polarization plots of the Cr–Co_xP and Co_xP electrodes in natural seawater.[33] Copyright © 2023 Wiley-VCH GmbH. (d) Schematic diagrams illustrating the mechanism of enhanced durability for NiFe@DG compared to NiFe/G. (e) Chronopotentiometry curves of NiFe@DG tested on nickel foams at a constant current density of 10 mA cm^{-2} in 1 M KOH + 1 M NaCl and 1 M KOH + seawater.[34] Copyright © 2023 American Chemical Society.

built-in electric field generated by the defective graphene coating at the electrode/electrolyte interface, which protected the core active NiFe alloy from dissolution and aggregation under harsh operating conditions.

3.3 Interface engineering

Interface engineering has been developed through the optimization of interfacial design between materials to significantly enhance the activity and stability of catalysts. On the one hand, the interface provides abundant active sites, facilitating electron transfer and reaction kinetics. On the other hand, interface-induced surface reconstruction and reaction mechanism modulation further reduce the reaction energy barriers. Additionally, interface engineering could be utilized to improve corrosion resistance and long-term stability of catalysts in high-salinity and corrosive environments by regulating the chemical environment and structural properties of the materials.[35–37]

As shown in Fig. 4, Li *et al.* utilized the advantage of graphdiyne (GDY),[38] which can grow on any substrate, to prepare a GDY/RhO_x/GDY bilayer heterostructure on RhO_x nanocrystals. This heterostructure formed an sp-hybridized carbon–rhodium oxide (sp-C–O-Rh) bilayer sandwich interface,

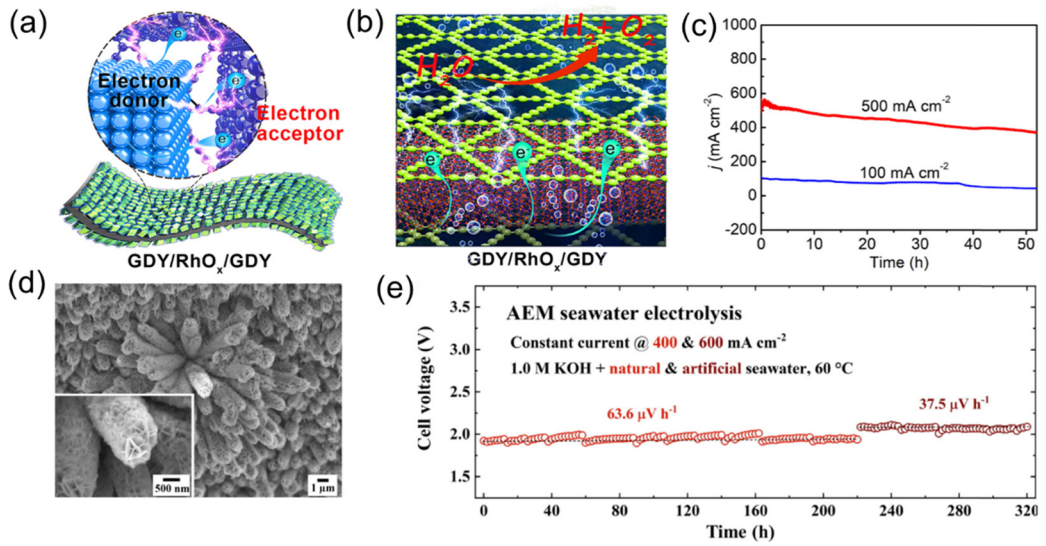

Fig. 4 (a) and (b) The efficient electron transfers from RhO_x to GDY and the electron-rich GDY surface. (c) Chronoamperometry test of GDY/RhO_x/GDY for overall seawater splitting at 500 and 100 mA cm^{-2}.[38] Copyright © 2022 National Academy of Sciences. (d) FE-SEM of (Ni,Fe)O(OH)@NiCoS. (e) Cell voltage durability profiles at 400 and 600 mA cm^{-2} feeding with alkaline seawater at 60 °C.[39] Copyright © 2023 Elsevier.

generating numerous active sites provided by the sp-C–O-Rh interface. The GDY/RhO_x/GDY demonstrated excellent catalytic performance and long-term stability, both in the OER and in full seawater decomposition. When used as both the cathode and anode to assemble a full seawater electrolyzer, the GDY/RhO_x/GDY structure required only 1.42 and 1.52 V *vs.* RHE to achieve current densities of 10 and 500 mA cm^{-2}, respectively. Additionally, at a current density of 100 mA cm^{-2}, the catalytic performance was maintained for over 53 hours without significant decay, demonstrating the catalyst's excellent long-term stability in seawater electrolysis. Shao *et al.* investigated a non-precious metal heterostructure catalyst (Ni,Fe)O(OH)@NiCoS Nas (Fig. 4d),[39] which was constructed on a nickel foam substrate using a "hydrothermal + annealing" synthesis strategy. This self-supporting electrode, used for seawater OER catalysis, featured a three-dimensional structure, abundant oxygen vacancies, and a heterojunction interface. An anion exchange membrane (AEM) full cell, composed of the non-precious metal OER electrode (Ni,Fe)O(OH)@NiCoS NAs/NF and the HER electrode NiFe LDHs@NiCoS NAs/NF, achieved stable operation in natural seawater for over 300 hours at 400 and 600 mA cm^{-2} (with voltage decay < 100 μV h^{-1}) (Fig. 4e). DFT calculations indicated that electronic transfer between the metal–oxygen sites of the catalyst and the core–shell structure promoted anodic reconstruction and regulated the OER reaction mechanism to a "M–O" dual-site lattice oxygen mechanism (LOM).

3.4 Constructing a Cl^- blocking layer

Constructing a Cl^- blocking layer is a crucial strategy for enhancing the stability and efficiency of catalysts in seawater electrolysis. This layer effectively prevents chloride ions from adsorbing onto the catalyst surface,[40–42] which can otherwise lead to competitive side reactions, corrosion, and performance degradation. By selectively allowing the transport of desired reactants while inhibiting chloride interference, the blocking layer enhances catalytic activity and extends the operational lifespan of the system. Additionally, it provides a protective barrier that mitigates structural damage caused by aggressive ions in saline environments, ensuring stable and efficient seawater splitting under harsh conditions.

Inspired by the concept of hard and soft acids and bases, Zhang *et al.* proposed an efficient surface anti-corrosion engineering strategy.[43] This involves constructing a $P_3O_{10}^{5-}$ polyoxyanion passivation layer on the surface of $Ni(OH)_2$, thereby enhancing the acidity of Ni sites to avoid erosion by soft base Cl^-. Molecular dynamics (MD) simulations further demonstrated that the surface $P_3O_{10}^{5-}$ oxyanions exhibit strong electrostatic repulsion against Cl^- ions, reducing the concentration of Cl^- near the electrode by nearly half, as is depicted in Fig. 5a–c. When $Ni(OH)_2$–$P_3O_{10}^{5-}$ was paired with Pt/C in an electrolyzer for alkaline seawater splitting, it achieved a current density of 1.4 A at 2.2 V, with a duration exceeding 240 hours. Sun *et al.* synthesized a CoFePBA/Co_2P anode with a Cap/Pin structure and applied it to an industrial-scale, highly efficient seawater electrolysis process.[44] The optimized electrode underwent reconstruction, generating PO_4^{3-} and $Fe(CN)_6^{3-}$ during

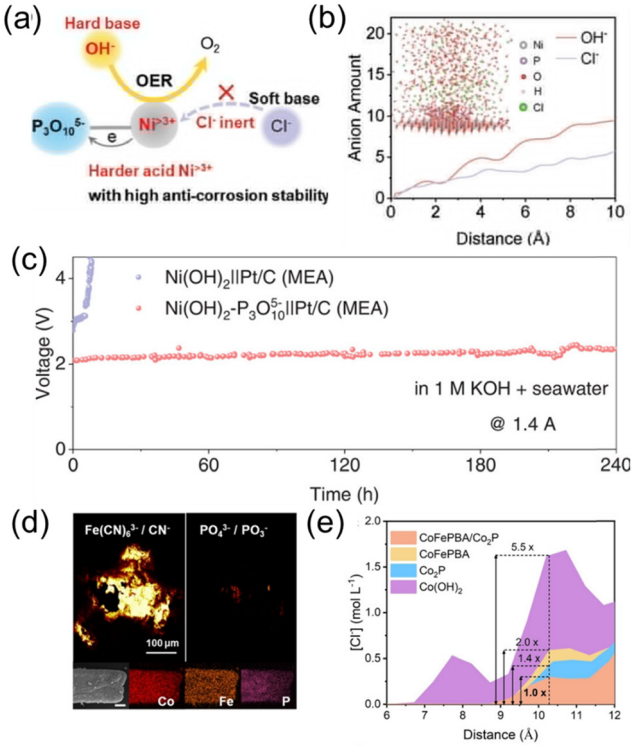

Fig. 5 (a) $P_3O_{10}^{5-}$ modification induces the formation of harder acid $Ni^{>3+}$ sites that are inert to soft base Cl^- based on the hard and soft acids and bases (HSAB) principle. It could suppress Cl^- attacking and prefer OH^- adsorption for the OER, thus enhancing the anti-corrosion ability. (b) The calculated amounts of OH^- and Cl^- above the $Ni(OH)_2$–$P_3O_{10}^{5-}$ electrode surface. The inset is the equilibrium configuration of the electrolyte system (1.0 M KOH + 0.5 M NaCl) above the electrode surface of $Ni(OH)_2$–$P_3O_{10}^{5-}$.[43] (c) Long-term durability test of the MEA flow electrolyzer assembled with $Ni(OH)_2$–$P_3O_{10}^{5-}$‖Pt/C and $Ni(OH)_2$‖Pt/C at 1.4 A in 1.0 M KOH + real seawater.[43] Copyright © 2024 Wiley-VCH GmbH. (d) TOF-SIMS mapping for $Fe(CN)_6^{3-}$/CN^- and PO_4^{3-}/PO_3^-, and EDX elemental mapping (scale bar: 20 μm) for Co, Fe and P of CoFePBA/Co_2P. (e) Profiles of Cl^- concentration as a function of position (distance) perpendicular to different samples.[44] Copyright © 2023 Wiley-VCH GmbH.

the OER process. It was found that PO_4^{3-} and $Fe(CN)_6^{3-}$ provided synergistic effects through electrostatic repulsion and dense coverage, respectively, imparting excellent anti-corrosion properties to the electrode. As a result, the CoFePBA/Co_2P electrode was able to catalyze the oxidation reaction of alkaline brine stably within the current density range of 200–2000 mA cm^{-2} for up to 1000 hours without corrosion issues, as shown in Fig. 5. Combined experimental tests and MD simulations showed that the Cl^- adsorption on the CoFePBA/Co_2P electrode was reduced by nearly 5.5 times compared to the $Co(OH)_2$ electrode. This synergistic interaction between ions can also be extended to other anion combinations (such as SO_4^{2-}/$Fe(CN)_6^{3-}$), exhibiting excellent corrosion resistance, thus confirming the universality of this strategy.

3.5 Biomass electrooxidation substituting the OER

Biomass electrooxidation, including the oxidation of glycerol, ethanol, and aldehydes, offers a promising alternative to the conventional OER at the anode.[17,23,45] This approach not only

significantly reduces the overpotential typically required for the OER, but also facilitates the production of value-added products. The oxidation of biomass compounds enables carbon-neutral energy generation while simultaneously producing valuable by-products, providing a sustainable solution for both energy production and chemical synthesis.[46–50]

Yuan *et al.* proposed a sea urchin-shaped Fe and Ni co-doped cobalt phosphide (FeNi–CoP/NF) supported on nickel foam for a hydrazine-assisted seawater electrolysis system.[51] The three-dimensional sea urchin-shaped nanostructure of FeNi–CoP/NF, combined with electronic structure and lattice strain engineering achieved through Fe and Ni co-doping, enhanced its bifunctional electrocatalytic capabilities. It achieved a current density of 10 mA cm^{-2} at low overpotentials of 36 mV for the HER and 236 mV for the HzOR. In the hydrazine-assisted seawater electrolysis system, with FeNi–CoP/NF as both the anode and cathode, only 580 mV was required to reach a current density of 1 A cm^{-2}, significantly lower than other alternatives. Furthermore, this catalyst achieved an industrial current density of 1.5 A cm^2 at an ultralow voltage of only 163 mV in the hydrazine hydrate-assisted seawater electrolysis system and was stable in seawater for several hundred hours, as is shown in Fig. 6.

Wang *et al.* synthesized partially hydroxylated rhodium metallenes with porous, ultrathin, defect-rich, and heterostructure features through a one-step hydrothermal method. The 2D ultrathin porous metallene structure promoted charge transfer, exposed active sites, and improved atomic utilization. The defect-rich and amorphous structure provided abundant active sites and facilitated mass transfer. The synergy between Rh and RhOOH optimized the adsorption and dissociation of substances, improving electrocatalytic performance. Additionally, the *in situ* reconstruction of Rh/RhOOH helped optimize surface catalytic centers, achieving stable catalytic reactions. As a bifunctional electrocatalyst for the HER and ethylene glycol oxidation reaction (EGOR), Rh/RhOOH metalenes exhibited excellent catalytic activity and stability. In the ethylene glycol-assisted seawater electrolysis system, Rh/RhOOH metallenes required only 0.678 V to achieve efficient hydrogen production at a current density of 10 mA cm^{-2}, significantly lower than traditional seawater electrolysis.[52]

4. The effect of Br^- on seawater electrolysis

Developing efficient and durable OER catalysts is an ideal method to improve the efficiency of direct seawater electrolysis for hydrogen production. However, these catalysts must meet supercritical survival requirements, especially under high current density and voltage conditions in pure seawater. Adding chlorine-free bases or salts to seawater electrolytes, along with commonly used high-activity OER catalysts, is a potential pathway to achieving industrial-scale green hydrogen production, although the corrosion problem caused by the ClOR remains unresolved. Combining the first two methods is the most feasible approach for large-scale green hydrogen production.

Except for Cl^-, Br^- primarily affects the anode by causing pitting. Recently, Lu *et al.* found that Br^- posed a greater threat to nickel-based anodes in seawater than Cl^-. Br^- has lower corrosion resistance and faster corrosion kinetics compared to Cl^-. Through experimental and simulation studies, they found that Cl^- tends to cause localized, deep, and narrow corrosion pits, while Br^- leads to widespread, shallow, and broad corrosion pits. This difference is attributed to fast diffusion of Cl^- and reduced

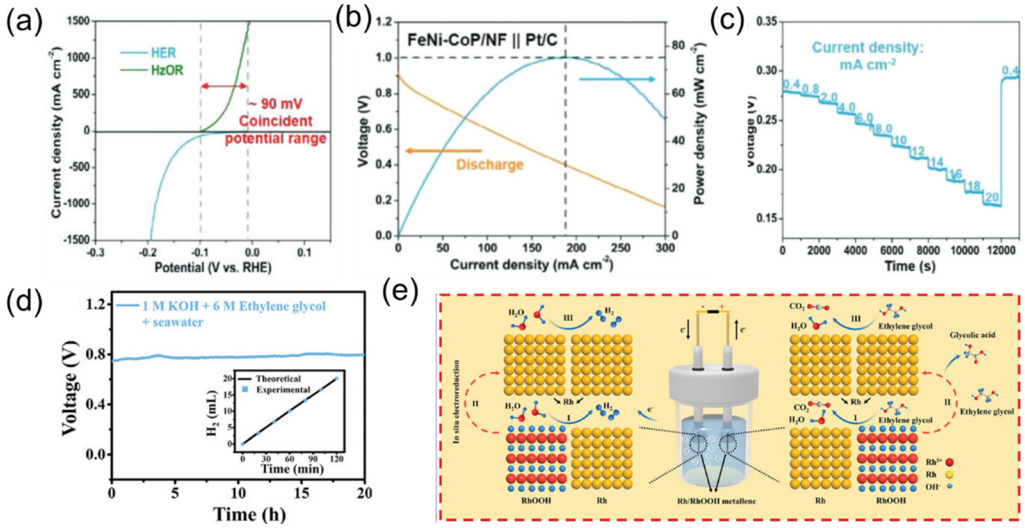

Fig. 6 (a) Polarization curves for conventional seawater electrolysis and hydrazine-assisted seawater electrolysis. (b) Discharge polarization curve and power density plots for the direct hydrazine fuel cell assembling FeNi–CoP/NF as the anode. (c) Galvanostatic discharge/charge curves at different current densities.[51] Copyright © 2024 Wiley-VCH GmbH. (d) Chronopotentiometry curves of Rh/RhOOH metallene‖Rh/RhOOH metallene at 10 mA cm^{-2} in 1 M KOH + 6 M EG + seawater solutions for 20 h. The inset in (d) illustrates the measured H_2 quantity and theoretical values at the cathode. (e) Mechanistic diagram of Rh/RhOOH metallene for hydrogen production *via* ethylene glycol-assisted seawater splitting.[52] Copyright © 2022 Wiley-VCH GmbH.

reaction energy of Br^- inside the passivation layer. Moreover, Br^- can also cause extensive delamination of the catalyst layer, accelerating performance degradation and severely damaging the integrity of nickel-based electrodes, as shown in Fig. 7a–c. This study emphasizes the importance of developing anodes that are resistant to both Cl^- and Br^- corrosion, marking significant progress toward the sustainable development of seawater electrolysis technology. Strategies to mitigate the impact of Cl^- on seawater electrolysis anode catalysts could also be applied to Br^-.[53]

5. The impacts of alkali metal and alkaline earth metal ions on seawater electrolysis

For alkaline cations like Na^+, Ca^{2+}, and Mg^{2+}, the focus is on reducing the adhesion of precipitates on the cathode catalyst by preparing highly hydrophobic electrocatalysts. In the process of direct seawater electrolysis, since the thermodynamic reduction potentials of cations such as Na^+, Mg^{2+}, and Ca^{2+} are much more negative than that of the HER,[56] competitive reactions on the cathode are less discussed compared to the anode. At the anode, OH^- is consumed at low current densities, transitioning to H_2O oxidation at high current densities, leading to a local drop in pH. At the cathode, the generation of OH^- increases pH, enhancing the thermodynamic potential of the HER and narrowing the potential gap between cation reduction and the HER, promoting cation electroreduction. These pH changes can lead to the formation of impurity layers on the electrode surface, hindering the transfer of water molecules and causing instability.[57–59]

For example, Amal *et al.* observed severe activity loss, and X-ray photoelectron spectroscopy (XPS) revealed a white layer of Na^+, Ca^{2+}, and Mg^{2+} salts, highlighting the challenges of

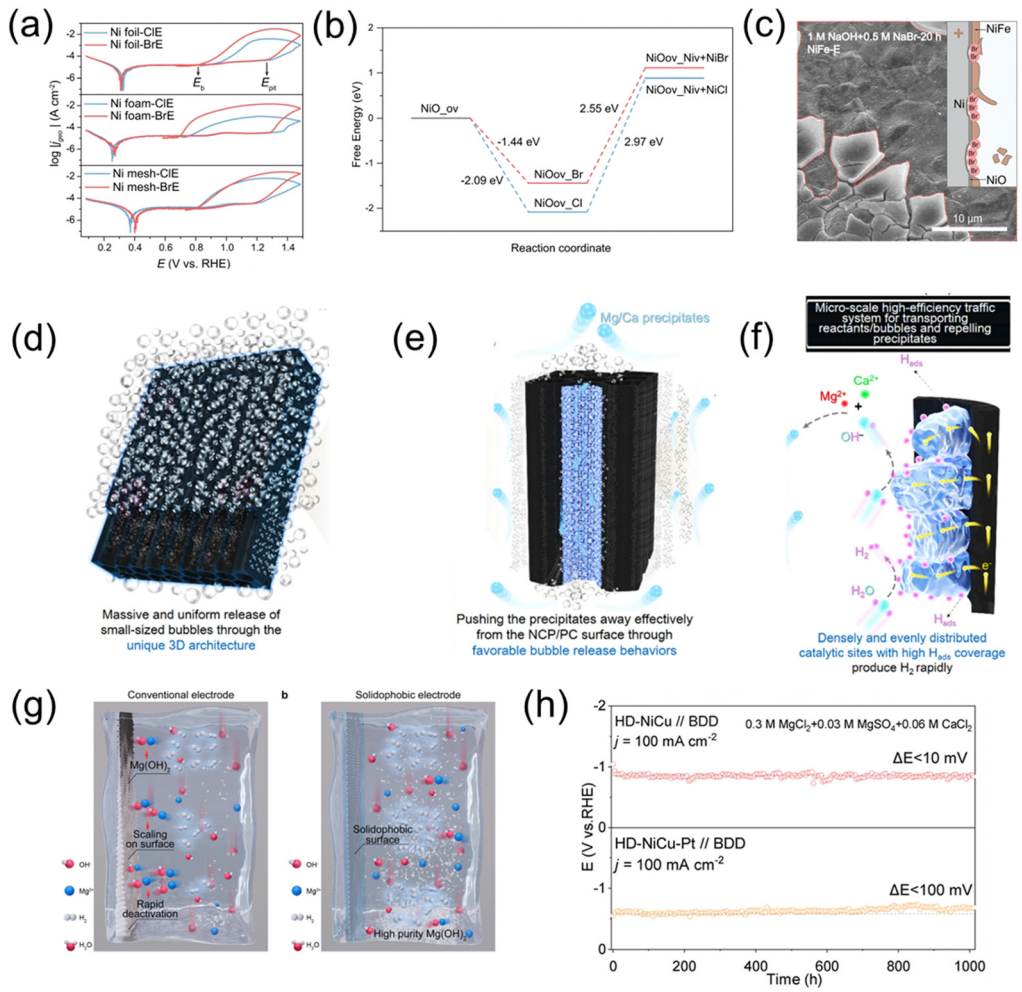

Fig. 7 (a) CPCs of Ni substrates tested in ClE and BrE at a scan rate of 10 mV s^{-1}. (b) Calculated free-energy diagrams for NiO corroded by halide, where ov denotes the oxygen vacancy and Niv denotes the Ni vacancy. (c) Corresponding SEM images of NiFe-E observed after 20 h operation in 1 M NaOH + 0.5 M NaBr.[53] Copyright © 2023 Springer Nature. (d)–(f) Schematic diagrams of efficient traffic of bubbles and precipitates on/in the NCP/CP. The bubble acts as the cleaner to make NCP/CP free from precipitation by repelling precipitates without a break.[54] Copyright © 2024 Springer Nature. (g) Schematic illustration of natural seawater electrolysis on a solidophobic cathode. (h) Long-term accelerated durability tests of the NiCu alloy and Pt–NiCu alloy electrode under 100 mA cm^{-2}.[55] Copyright © 2024 American Chemical Society.

natural seawater.[60] Furthermore, the pH changes during operation can cause the anode to become acidic and the cathode alkaline, promoting the formation of insoluble precipitates such as MgO and $Ca(OH)_2$ on the electrode surface. This issue extends from the cathode to the anode and membrane, where metal ions can increase charge transfer resistance and reduce the reaction rate, lowering seawater electrolysis efficiency. Additionally, microorganisms in seawater can precipitate and adhere to the electrode and membrane surfaces, further obstructing charge transfer and water diffusion, exacerbating the problem. There are two main approaches to enhance the anti-scaling capability of cathode catalysts: (1) modifying the electrode to improve anti-scaling properties and (2) using electrolyzer engineering.

5.1 Enhanced electrode anti-precipitation capability

By constructing mass transport channels on the surface of cathode catalysts, a rapid pathway is provided for the transport of bubbles, fluids, and precipitates, which helps prevent their accumulation on the electrode surface and accelerates the HER mass transport steps. Additionally, this initiative contributes to long-term hydrogen evolution stability under high potential conditions. For example, Sun *et al.* studied a highly efficient anti-scaling seawater electrolysis catalyst—a microbubble/precipitate transport system (MBPTS), which achieves stable alkaline and natural seawater reduction electrolysis by constructing a honeycomb-like 3D cathode. The researchers uniformly distributed NiCoP nanostructures on a porous carbon framework to prepare an NCP/PC electrode with high activity and stability (Fig. 7d–f).

The NCP/PC electrode's unique 3D structure and microscale transport system allow for the uniform release of bubbles, moderate migration speed, and effective prevention of precipitate accumulation, improving electrolysis efficiency. In alkaline seawater, the NCP/PC electrode maintained a low overpotential of 160 mV at a current density of 1 A cm^{-2} for 1000 hours, demonstrating exceptional stability. In natural seawater, the NCP/PC electrode exhibited the highest anti-scaling capability, with evenly distributed and small-sized released bubbles that effectively pushed magnesium and calcium precipitates away from the electrode surface, preventing the active sites from being blocked. The performance of the NCP/PC electrode outperformed other metal phosphide electrodes, such as CoP/PC and Ni_2P/PC, showcasing superior hydrogen evolution activity and anti-scaling ability. Moreover, in a flow electrolyzer, the NCP/PC electrode operated stably for 150 hours at a current density of 500 mA cm^{-2}, maintaining nearly 100% faradaic efficiency for H_2 production.[54] Lu *et al.* addressed the critical issue of cathode scaling in direct seawater electrolysis by developing a hydrophobic electrode composed of NiCu alloys,[55] which can be seen in Fig. 7g and h. This electrode demonstrated over 1000 hours of stable performance in high-salinity solutions rich in Mg^{2+} and Ca^{2+}. More importantly, in addition to hydrogen production, the hydrophobic electrode simultaneously facilitated the production of high-purity magnesium hydroxide. Experimental results, supported by AIMD simulations, revealed that the high surface disorder of the NiCu alloy contributed to the formation of a dense hydrated layer, which effectively inhibited the non-uniform nucleation of magnesium ions on the electrode surface.

5.2 Electrolyzer engineering

In seawater electrolysis, electrolyzer engineering plays a critical role in addressing challenges such as anion corrosion and cation precipitation. The use of membranes or specialized electrolyzer design that inhibit the precipitation of unwanted cations can maintain the stability and efficiency of the electrolysis process. These engineering solutions ensure longer operational lifetimes for the electrolyzer, minimize maintenance requirements, and enhance the overall performance of seawater electrolysis for sustainable hydrogen production.[18,61,62]

As depicted in Fig. 8a–c, Li *et al.* designed a pH-asymmetric electrolyzer that employs a Na^+-exchange membrane for direct seawater electrolysis,[63] effectively preventing Cl^- corrosion and Ca^{2+}/Mg^{2+} precipitation while utilizing the chemical potential difference between different electrolytes to reduce the required voltage. *In situ* Raman spectroscopy and density functional theory calculations revealed that the atomically dispersed Pt catalyst based on Ni–Fe–P nanowires can lower the energy barrier by 0.26 eV, promoting the hydrolysis reaction in seawater and accelerating hydrogen evolution kinetics. As a result, this asymmetric electrolyzer exhibited current densities of 10 mA cm^{-2} and 100 mA cm^{-2} at voltages of 1.31 V and 1.46 V, respectively. At 80 °C, it was also able to achieve a current density of 400 mA cm^{-2} at a low voltage of 1.66 V, corresponding to an electricity cost of $1.36 per kilogram of hydrogen, which is below the U.S. Department of Energy's target for 2025. Xie *et al.* approached the challenges faced by direct seawater electrolysis for hydrogen production from a novel perspective that combines physical mechanics and electrochemistry.[64] They creatively pioneered a new principle and technology for *in situ* direct electrolysis of seawater without desalination, completely isolating seawater ions to achieve efficient hydrogen production without desalination processes, side reactions, or additional energy consumption (essentially treating seawater as pure water for direct *in situ* electrolysis).

Their pioneering research innovatively integrated molecular diffusion, interfacial phase equilibrium, and other physicochemical processes with electrochemical reactions, establishing a comprehensive theoretical framework for phase-transition-driven seawater direct electrolysis in hydrogen production. This advanced model unveils the mechanistic influence of interfacial pressure differences on spontaneous phase transition mass transfer within micro-scale gas gap pathways, enabling the development of a dynamically self-regulating and stable electrolysis system that synergistically couples electrochemical reactions with seawater mass transport. This approach effectively resolves the longstanding challenge of corrosive degradation, which has impeded progress in seawater electrolysis for hydrogen production over the past five decades. Furthermore, the research team successfully engineered the world's first 400 L h^{-1} seawater *in situ* direct electrolysis technology and equipment for hydrogen production. Demonstrating exceptional durability and performance, this system has achieved uninterrupted operation

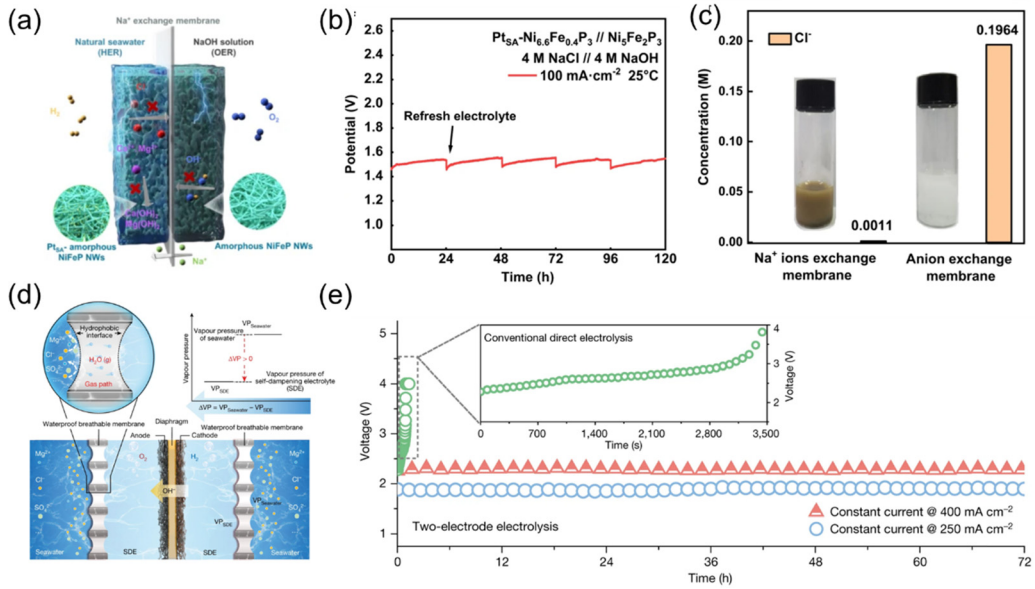

Fig. 8 (a) Scheme for the asymmetric electrolyzer with sodium ion exchange membrane. (b) Long-term stability test of the asymmetric electrolyzer at constant 100 mA cm^{-2}. (c) Concentration of Cl^- ions in anode electrolytes for asymmetric electrolyzers with a Na^+/anion exchange membrane and the photographs after adding $AgNO_3$ solution (inset).[63] Copyright © 2023 Springer Nature. (d) The liquid–gas–liquid phase transition-based migration mechanism of the water purification and migration process and the driving force. (e) Electrolysis durability test at constant current densities of 250 mA cm^{-2} and 400 mA cm^{-2} in Shenzhen Bay seawater for a total period of 72 h. The inset shows the electrolysis durability test of conventional direct seawater splitting using commercial electrocatalysts.[64] Copyright © 2022 Nature.

for over 3200 hours in the highly corrosive environment of Shenzhen Bay seawater, showcasing a robust and scalable hydrogen production process. Importantly, the underlying principles and technological framework can be extended to enable direct *in situ* hydrogen production from diverse water resources, including river water, wastewater, and saline lakes. This breakthrough not only offers new opportunities for resource utilization and renewable energy generation but also provides a transformative solution to global energy and environmental challenges (Fig. 8d and e).

6. Conclusions

This work provides an in-depth investigation into the challenges and opportunities associated with electrocatalytic seawater splitting for hydrogen production. By elucidating the electrochemical processes and the adverse effects of seawater's complex ionic composition on catalytic activity and stability, this study highlights the critical need for advanced electrocatalysts tailored to the unique conditions of seawater electrolysis. Strategies to mitigate ionic interference, such as the rational design of selective catalysts and innovative system architectures, are discussed as pathways to enhance efficiency and operational durability for seawater splitting hydrogen production. Future efforts should focus on integrating these advancements with renewable energy resources to achieve large-scale, sustainable hydrogen production. Additionally, addressing long-term issues such as electrode degradation, chlorine evolution suppression, and energy efficiency optimization will be pivotal in advancing the industrialization of seawater electrolysis. This work establishes a foundation for further research aimed at overcoming the remaining technical barriers and unlocking the full potential of seawater electrolysis as a cornerstone technology for green hydrogen production. However, future research and advancements should be focused on the following directions:

(1) In addition to the influence of Cl^- and Br^- on the anode for seawater electrolysis, other oxygen-containing anions such as SO_4^{2-}, NO_3^-, and PO_4^{3-} can resist the corrosive effects of Cl^- and Br^- on the anode electrocatalyst. However, these anions simultaneously reduce the adsorption of OH^-, affecting the seawater splitting performance. Therefore, there is an urgent need to find a more effective approach to balance this adsorption process on the anode electrocatalysts.

(2) The utilization of biomass electrooxidation as an alternative to the OER not only decreases the overall energy consumption and cost associated with electrolytic seawater treatment, but also enables the production of high-value chemicals. Nevertheless, it is imperative to evaluate the operational costs related to producing these high-value chemicals within the electrolytic cell. These chemicals primarily consist of alcohols, aldehydes, acids, and other organic compounds, many of which exhibit viscous liquid properties.

(3) Currently, the predominant technical approach involves indirect seawater electrolysis, which entails a pre-desalination process followed by alkaline water electrolysis for hydrogen production. The integration of seawater desalination systems with alkaline electrolytic water hydrogen production technology is relatively advanced and can rapidly achieve large-scale

industrialization. However, it is crucial to consider the costs associated with the seawater desalination system, improvements in catalysts for alkaline electrolytic cells, and electrolytic efficiency. The primary focus should be on reducing comprehensive energy consumption and technical costs related to hydrogen production. Direct seawater electrolysis for hydrogen production is still in its early stages, but if advancements are made in key areas such as industrial design of electrolytic cells, pilot testing of electrolytic equipment, and long-term verification of system stability and service life, this technology holds immense potential for the future.

Data availability

The data that support the findings of this study are available from the corresponding author upon reasonable request.

Conflicts of interest

There are no conflicts to declare.

Acknowledgements

The authors are grateful for the financial support from the National Natural Science Foundation of China (52472231 and 52311530113), the Science and Technology Commission of Shanghai Municipality (22DZ1205600), and the Central Guidance on Science and Technology Development Fund of Zhejiang Province (2024ZY01011).

References

1 B. Lee, L. Wang, Z. Wang, N. J. Cooper and M. Elimelech, *Energy Environ. Sci.*, 2023, **16**, 714–722.
2 K. Zuo, W. Wang, A. Deshmukh, S. Jia, H. Guo, R. Xin, M. Elimelech, P. M. Ajayan, J. Lou and Q. Li, *Nat. Nanotechnol.*, 2020, **15**, 1025–1032.
3 D. J. Lampert, H. Cai and A. Elgowainy, *Energy Environ. Sci.*, 2016, **9**, 787–802.
4 R. R. Beswick, A. M. Oliveira and Y. Yan, *ACS Energy Lett.*, 2021, **6**, 3167–3169.
5 C. He, Z. Liu, J. Wu, X. Pan, Z. Fang, J. Li and B. A. Bryan, *Nat. Commun.*, 2021, **12**, 4667.
6 M. A. Khan, T. Al-Attas, S. Roy, M. M. Rahman, N. Ghaffour, V. Thangadurai, S. Larter, J. Hu, P. M. Ajayan and M. G. Kibria, *Energy Environ. Sci.*, 2021, **14**, 4831–4839.
7 X.-L. Zhang, P.-C. Yu, X.-Z. Su, S.-J. Hu, L. Shi, Y.-H. Wang, P.-P. Yang, F.-Y. Gao, Z.-Z. Wu, L.-P. Chi, Y.-R. Zheng and M.-R. Gao, *Sci. Adv.*, 2023, **9**, eadh2885.
8 S. Dresp, F. Dionigi, M. Klingenhof and P. Strasser, *ACS Energy Lett.*, 2019, **4**, 933–942.
9 S. Dresp, T. Ngo Thanh, M. Klingenhof, S. Brückner, P. Hauke and P. Strasser, *Energy Environ. Sci.*, 2020, **13**, 1725–1729.
10 X.-L. Zhang, P.-C. Yu, S.-P. Sun, L. Shi, P.-P. Yang, Z.-Z. Wu, L.-P. Chi, Y.-R. Zheng and M.-R. Gao, *Nat. Commun.*, 2024, **15**, 9462.
11 H. Hu, Z. Zhang, L. Liu, X. Che, J. Wang, Y. Zhu, J. P. Attfield and M. Yang, *Sci. Adv.*, 2024, **10**, eadn7012.
12 Z. Pu, J. Zhao, I. S. Amiinu, W. Li, M. Wang, D. He and S. Mu, *Energy Environ. Sci.*, 2019, **12**, 952–957.
13 Y. Liu, J. Cai, W. Zhang, J. Hao, Y. Zhou, X. Pan and H. Zhu, *Chem. Commun.*, 2025, **61**, 3195–3198.
14 Q. Huang, B. Xia, M. Li, H. Guan, M. Antonietti and S. Chen, *Nat. Commun.*, 2024, **15**, 4157.
15 P.-C. Yu, X.-L. Zhang, T.-Y. Zhang, X.-Y.-N. Tao, Y. Yang, Y.-H. Wang, S.-C. Zhang, F.-Y. Gao, Z.-Z. Niu, M.-H. Fan and M.-R. Gao, *J. Am. Chem. Soc.*, 2024, **146**, 20379–20390.
16 F. Dionigi, T. Reier, Z. Pawolek, M. Gliech and P. Strasser, *ChemSusChem*, 2016, **9**, 962–972.
17 J. Huang, B. Hu, J. Meng, T. Meng, W. Liu, Y. Guan, L. Jin and X. Zhang, *Energy Environ. Sci.*, 2024, **17**, 1007–1045.
18 G. A. Lindquist, Q. Xu, S. Z. Oener and S. W. Boettcher, *Joule*, 2020, **4**, 2549–2561.
19 X. Kang, F. Yang, Z. Zhang, H. Liu, S. Ge, S. Hu, S. Li, Y. Luo, Q. Yu, Z. Liu, Q. Wang, W. Ren, C. Sun, H.-M. Cheng and B. Liu, *Nat. Commun.*, 2023, **14**, 3607.
20 X. Liu, M. Gong, D. Xiao, S. Deng, J. Liang, T. Zhao, Y. Lu, T. Shen, J. Zhang and D. Wang, *Small*, 2020, **16**, 2000663.
21 Z. Yu and L. Liu, *Adv. Mater.*, 2023, **36**, 2308647.
22 K. Hemmati, A. Kumar, A. R. Jadhav, O. Moradlou, A. Z. Moshfegh and H. Lee, *ACS Catal.*, 2023, **13**, 5516–5528.
23 Q. Mao, K. Deng, H. Yu, Y. Xu, Z. Wang, X. Li, L. Wang and H. Wang, *Adv. Funct. Mater.*, 2022, **32**, 2201081.
24 L. Guo, J. Chi, J. Zhu, T. Cui, J. Lai and L. Wang, *Appl. Catal., B*, 2023, **320**, 121977.
25 W. H. Hung, B. Y. Xue, T. M. Lin, S. Y. Lu and I. Y. Tsao, *Mater. Today Energy*, 2021, **19**, 100575.
26 K. Jiang, W. Liu, W. Lai, M. Wang, Q. Li, Z. Wang, J. Yuan, Y. Deng, J. Bao and H. Ji, *Inorg. Chem.*, 2021, **60**, 17371–17378.
27 Y. Long, P. Jiang, P. Liao, C. Yang, S. Li, J. Xian, Y. Sun, Q. Liu and G. Li, *Small*, 2024, **20**, 2403991.
28 L.-W. Shen, Y. Wang, J.-B. Chen, G. Tian, K.-Y. Xiong, C. Janiak, D. Cahen and X.-Y. Yang, *Nano Lett.*, 2023, **23**, 1052–1060.
29 G. Wang, W. Tang, Y. Chen, P. Ji, M. Lu, H. Wei, L. Cui, X. Chen and G. Wang, *Adv. Funct. Mater.*, 2024, **34**, 2404470.
30 D. Liu, X. Wei, J. Lu, X. Wang, K. Liu, Y. Cai, Y. Qi, L. Wang, H. Ai and Z. Wang, *Adv. Mater.*, 2024, **36**, 2408982.
31 J. Wang, W. He, Y. Zong, Y. Tang, J. Wang and R. Ma, *Chem. Commun.*, 2024, **60**, 9444–9447.
32 Y. Li, S. Zuo, Q. Li, H. Huang, X. Wu, J. Zhang, H. Zhang and J. Zhang, *Appl. Catal., B*, 2022, **318**, 121832.
33 Y. Song, M. Sun, S. Zhang, X. Zhang, P. Yi, J. Liu, B. Huang, M. Huang and L. Zhang, *Adv. Funct. Mater.*, 2023, **33**, 2214081.
34 Z. Gong, J. Liu, M. Yan, H. Gong, G. Ye and H. Fei, *ACS Nano*, 2023, **17**, 18372–18381.
35 S. Liu, Z. Zhang, K. Dastafkan, Y. Shen, C. Zhao and M. Wang, *Nat. Commun.*, 2025, **16**, 773.
36 L.-L. Ma, Y.-R. Hao, J. Sun, Y. Chen, C. Li, H. Xue, J. Sun, Q. Wang and L. Wu, *Adv. Funct. Mater.*, 2025, **35**, 2570050.
37 H. Zhu, J. J. Wang, Z. Xu, Y. Tan and J. Wang, *Small*, 2024, **20**, 2404919.
38 Y. Gao, Y. Xue, F. He and Y. Li, *Proc. Natl. Acad. Sci. U. S. A.*, 2022, **119**, e2206946119.
39 J. Na, H. Yu, S. Jia, J. Chi, K. Lv, T. Li, Y. Zhao, Y. Zhao, H. Zhang and Z. Shao, *J. Energy Chem.*, 2024, **91**, 370–382.
40 J. Sun, S. Zhou, Z. Zhao, S. Qin, X. Meng, C.-H. Tung and L.-Z. Wu, *Energy Environ. Sci.*, 2025, **18**, 1952–1962.
41 T. Ma, W. Xu, B. Li, X. Chen, J. Zhao, S. Wan, K. Jiang, S. Zhang, Z. Wang, Z. Tian, Z. Lu and L. Chen, *Angew. Chem., Int. Ed.*, 2021, **60**, 22740–22744.
42 J. Li, Y. Liu, H. Chen, Z. Zhang and X. Zou, *Adv. Funct. Mater.*, 2021, **31**, 2101820.
43 X. Wang, H. Hu, J. Song, J. Ma, H. Du, J. J. Wang, M. Wang, W. Chen, Y. Zhou, J. Wang, M. Yang and L. Zhang, *Adv. Energy Mater.*, 2024, **15**, 2402883.
44 W. Liu, J. Yu, M. G. Sendeku, T. Li, W. Gao, G. Yang, Y. Kuang and X. Sun, *Angew. Chem., Int. Ed.*, 2023, **62**, e202309882.
45 B. Zhao, J.-W. Liu, Y.-R. Yin, D. Wu, J.-L. Luo and X.-Z. Fu, *J. Mater. Chem. A*, 2019, **7**, 25878–25886.
46 L. Zhang, Z. Wang and J. Qiu, *Adv. Mater.*, 2022, **34**, 2109321.
47 K. Yang, M. Li, T. Gao, G. Xu, D. Li, Y. Zheng, Q. Li and J. Duan, *Nat. Commun.*, 2024, **15**, 7060.
48 T. Wang, Y. Yuan, W. Shi, L. Gai, R. Peng, J. Li, Z. Kang and X. Tian, *Chem. Commun.*, 2025, **61**, 1719–1728.
49 Y. Feng, N. Ran, X. Wang, Q. Liu, J. Wang, L. Liu, K. Suenaga, W. Zhong, R. Ma and J. Liu, *Adv. Energy Mater.*, 2023, **13**, 2302452.
50 Y. Feng, X. Wang, J. Ma, N. Wang, Q. Liu, K. Suenaga, W. Chen, J. Zhang, Y. Zhou and J. Wang, *Adv. Energy Mater.*, 2024, **14**, 2401501.

51 H.-Y. Wang, F. Yan, H. Wang, S. Zhai, J.-T. Ren, L. Wang, M. Sun and Z.-Y. Yuan, *Adv. Energy Mater.*, 2024, **14**, 2402611.
52 Q. Mao, K. Deng, H. Yu, Y. Xu, Z. Wang, X. Li, L. Wang and H. Wang, *Adv. Funct. Mater.*, 2022, **32**, 2201081.
53 S. Zhang, Y. Wang, S. Li, Z. Wang, H. Chen, L. Yi, X. Chen, Q. Yang, W. Xu, A. Wang and Z. Lu, *Nat. Commun.*, 2023, **14**, 4822.
54 J. Liang, Z. Cai, Z. Li, Y. Yao, Y. Luo, S. Sun, D. Zheng, Q. Liu, X. Sun and B. Tang, *Nat. Commun.*, 2024, **15**, 2950.
55 L. Yi, X. Chen, Y. Wen, H. Chen, S. Zhang, H. Yang, W. Li, L. Zhou, B. Xu, W. Xu, W. Guan, S. Dai and Z. Lu, *Nano Lett.*, 2024, **24**, 5920–5928.
56 A. J. Esswein, Y. Surendranath, S. Y. Reece and D. G. Nocera, *Energy Environ. Sci.*, 2011, **4**, 499–504.
57 P. Farràs, P. Strasser and A. J. Cowan, *Joule*, 2021, **5**, 1921–1923.
58 H. Jin, X. Liu, A. Vasileff, Y. Jiao, Y. Zhao, Y. Zheng and S.-Z. Qiao, *ACS Nano*, 2018, **12**, 12761–12769.
59 Y. Lin, K. Sun, X. Chen, C. Chen, Y. Pan, X. Li and J. Zhang, *J. Energy Chem.*, 2021, **55**, 92–101.
60 X. Lu, J. Pan, E. Lovell, T. H. Tan, Y. H. Ng and R. Amal, *Energy Environ. Sci.*, 2018, **11**, 1898–1910.
61 W. Zang, T. Sun, T. Yang, S. Xi, M. Waqar, Z. Kou, Z. Lyu, Y. P. Feng, J. Wang and S. J. Pennycook, *Adv. Mater.*, 2020, **33**, 2003846.
62 W. Zheng, L. Y. S. Lee and K.-Y. Wong, *Nanoscale*, 2021, **13**, 15177–15187.
63 H. Shi, T. Wang, J. Liu, W. Chen, S. Li, J. Liang, S. Liu, X. Liu, Z. Cai, C. Wang, D. Su, Y. Huang, L. Elbaz and Q. Li, *Nat. Commun.*, 2023, **14**, 3934.
64 H. Xie, Z. Zhao, T. Liu, Y. Wu, C. Lan, W. Jiang, L. Zhu, Y. Wang, D. Yang and Z. Shao, *Nature*, 2022, **612**, 673–678.

